LETTER

doi:10.1038/nature12155

Psl trails guide exploration and microcolony formation in *Pseudomonas aeruginosa* biofilms

Kun Zhao[1]*, Boo Shan Tseng[2]*, Bernard Beckerman[3], Fan Jin[4], Maxsim L. Gibiansky[1], Joe J. Harrison[2], Erik Luijten[3,5], Matthew R. Parsek[2] & Gerard C. L. Wong[1,6,7]

Bacterial biofilms are surface-associated, multicellular, morphologically complex microbial communities[1–7]. Biofilm-forming bacteria such as the opportunistic pathogen *Pseudomonas aeruginosa* are phenotypically distinct from their free-swimming, planktonic counterparts[7–10]. Much work has focused on factors affecting surface adhesion, and it is known that *P. aeruginosa* secretes the Psl exopolysaccharide, which promotes surface attachment by acting as 'molecular glue'[11–15]. However, how individual surface-attached bacteria self-organize into microcolonies, the first step in communal biofilm organization, is not well understood. Here we identify a new role for Psl in early biofilm development using a massively parallel cell-tracking algorithm to extract the motility history of every cell on a newly colonized surface[16]. By combining this technique with fluorescent Psl staining and computer simulations, we show that *P. aeruginosa* deposits a trail of Psl as it moves on a surface, which influences the surface motility of subsequent cells that encounter these trails and thus generates positive feedback. Both experiments and simulations indicate that the web of secreted Psl controls the distribution of surface visit frequencies, which can be approximated by a power law. This Pareto-type[17] behaviour indicates that the bacterial community self-organizes in a manner analogous to a capitalist economic system[18], a 'rich-get-richer' mechanism of Psl accumulation that results in a small number of 'elite' cells becoming extremely enriched in communally produced Psl. Using engineered strains with inducible Psl production, we show that local Psl concentrations determine post-division cell fates and that high local Psl concentrations ultimately allow elite cells to serve as the founding population for initial microcolony development.

The extracellular matrix of *P. aeruginosa* biofilms is composed mostly of exopolysaccharides, proteins and DNA[19–21]. Biofilms formed by non-mucoid isolates of *P. aeruginosa* primarily use two types of exopolysaccharide: Psl and Pel[22]. To initiate biofilm development, the wild-type strain PAO1 uses Psl to promote adhesion of cells to surfaces[14,15]. Once associated with a surface, *P. aeruginosa* can remain fixed at the point of attachment or move. Formation of microcolonies (aggregates of ~50 cells or less) is the first step in the communal organization of a biofilm; however, little is known regarding the transition of individual cells to these discrete microcolonies[3–5,23].

Consistent with the role of Psl in surface adhesion[7,24], the average surface residence time of a PAO1 Δ*pslD* mutant strain (which cannot produce Psl) was 35 ± 10% shorter than that of wild type. Tracking algorithms allow us to isolate differences in spatial characteristics of cell–surface interactions, in addition to temporal characteristics such as residence time. We observed a fundamental difference in surface exploration patterns between the wild-type and Δ*pslD* strains (Fig. 1a–d and Supplementary Video 1) when we tracked the motility history of all cells in a 67 μm × 67 μm field of view (>700,000 images of individual cells, 11 h of data, time resolution of 3 s per frame). In Fig. 1a–d, black regions represent 'untouched' surface areas, whereas red regions represent areas visited by bacteria. For wild type, the surface coverage increased slowly to a maximum of ~55 ± 5% in 5 h. In contrast, the Δ*pslD* mutant covered 79 ± 10% in 5 h. These observed differences are not due to differences in growth between strains (Supplementary Fig. 1). To confirm that changes in surface motility, rather than changes in the numbers of bacteria visiting the surface, are responsible for these observations, we also compared wild type and Δ*pslD* at the same total number of bacterial visits (that is, the sum of the number of bacteria in all frames, $N_s = \sum n_i$, where n_i is the number of bacteria in frame i; Supplementary Fig. 2). Indeed, essentially the same trend was observed, with a surface coverage of 52 ± 4% for wild type at N_s = 124,000 and a surface coverage of 83 ± 10% for Δ*pslD* at the same N_s. These are averages from at least three replicates (Supplementary Methods).

Because Psl is important in both surface motility and adhesion, we characterized its spatial distribution with respect to bacterial trajectories. A TRITC-conjugated, Psl-specific lectin[12] was used to visualize Psl. We allowed wild-type cells to traverse a surface for 2 h before lectin staining and found that a trail of Psl was left on the surface (Supplementary Fig. 3). We verified that extracellular DNA[21] was not found in the trails (by staining with propidium iodide (data not shown) and SYTO 9 (Supplementary Figs 4 and 5)).

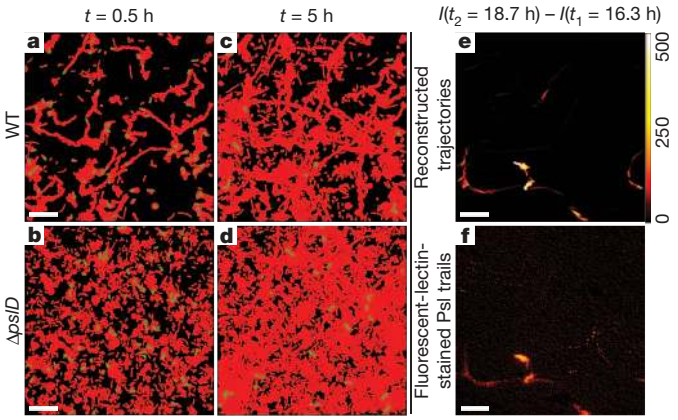

Figure 1 | Efficiency of surface coverage by bacterial trajectories and correlation with Psl trails. **a**–**d**, Cumulative surface coverage at 0.5 h (**a**, **b**) and 5 h (**c**, **d**). Red and black colours indicate traversed (that is, covered by bacterial trajectories) and fresh surface, respectively. Bacteria in the frame at the specified time points are shown in green. **e**, Reconstructed bacterial trajectories of wild type generated between 16.3 and 18.7 h after inoculation (colour scale indicates the time a given cell spent at each point). **f**, Psl trail left behind by bacteria in the same period, stained by fluorescently conjugated *Hippeastrum* hybrid (amaryllis) lectin. Scale bars, 10 μm.

[1]Department of Bioengineering, University of California, Los Angeles, California 90095, USA. [2]Department of Microbiology, University of Washington, Seattle, Washington 98195, USA. [3]Department of Materials Science and Engineering, Northwestern University, Evanston, Illinois 60208, USA. [4]CAS Key Laboratory of Soft Matter Chemistry, University of Science and Technology of China, Hefei, Anhui 230026, China. [5]Department of Engineering Sciences and Applied Mathematics, Northwestern University, Evanston, Illinois 60208, USA. [6]Department of Chemistry and Biochemistry, University of California, Los Angeles, California 90095, USA. [7]California NanoSystems Institute, University of California, Los Angeles, California 90095, USA.
*These authors contributed equally to this work.

Cell-tracking algorithms and lectin staining were combined to investigate the spatiotemporal aspects of Psl deposition in a manner that accounts for the changing speeds (and, therefore, local residence times) of cells. Figure 1e shows bacterial trajectories between times t_1 (16.3 h after inoculation) and t_2 (18.7 h after inoculation). Figure 1f shows the lectin-stained Psl trails generated in this time period (Methods and Supplementary Fig. 6). Surface regions with the brightest fluorescence signals and, hence, the highest local surface concentrations of Psl corresponded to those with the longest bacterial visits. Multiple visits to a surface region by different cells and extended residence times of a specific cell on the same surface region both served to increase local Psl concentration.

We used cell-tracking algorithms to determine the bacterial visit frequency for each surface pixel for the entire community (Methods). A surface visit map (Fig. 2a) of all wild-type cells within the field of view (Fig. 2b, ~15.7 h after inoculation) shows that a considerable fraction of the surface was never visited. Of the surface areas traversed by bacteria, most were traversed once. In fact, the visit frequency distribution (histogram of the number of pixels with N bacterial visits) was measured to be a monotonically decreasing function of N. The precise form of the function is complex; however, for values of N ranging from a few visits to more than a hundred visits, the distribution is approximately described by a power law with an exponent of -2.9 ± 0.1 (Fig. 2c), which serves as a simple metric for the distribution.

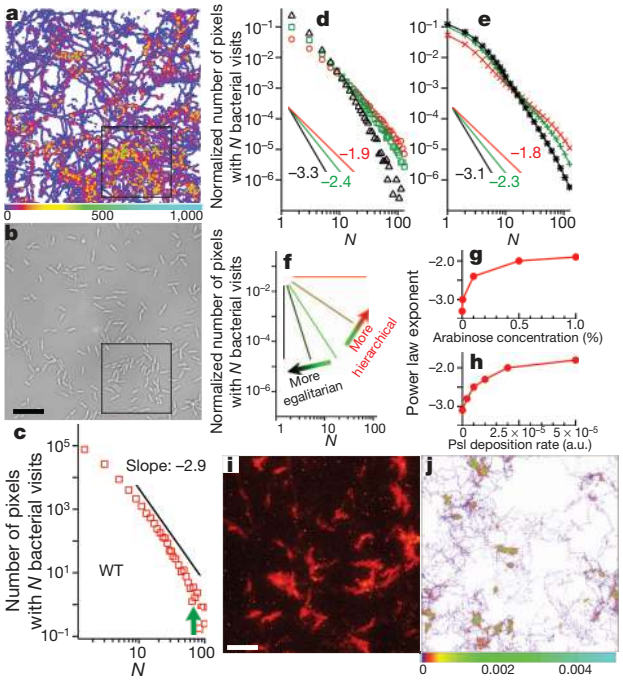

Figure 2 | Visit frequency distribution and its effect on bacterial movement. **a**, Visit frequency map of wild type for the first 15.7 h after inoculation, when microcolonies were just starting to form (example outlined by black square). **b**, Bright-field image for wild type at $t \approx 15.7$ h. **c**, Visit frequency distribution from **a**. The solid line shows a power-law decay with exponent −2.9. The green arrow indicates where the curve begins to deviate from this power law. **d**, Visit frequency distributions for $\Delta P_{psl}/P_{BAD}$-*psl* at arabinose concentrations of 0% (triangles), 0.1% (squares) and 1% (circles). **e**, Simulation results of visit frequency distributions at Psl deposition rates of 0 (asterisks), 10^{-5} (pluses), 5×10^{-5} (crosses) (arbitrary units; see Supplementary Methods). In **d** and **e**, each data set is normalized by the total number of visits (roughly the same as for **a**) and solid lines show power-law decay, labelled by exponent. **f**, Schematic graph showing that distributions with steep slopes are more egalitarian, whereas those with shallow slopes are more hierarchical. **g**, **h**, Fitted power-law exponents of visit frequency distributions from experiments at different arabinose concentrations (**g**) and simulations at different Psl deposition rates (**h**). **i**, A lectin-stained image showing hierarchical distribution of Psl ($\Delta P_{psl}/P_{BAD}$-*psl* at 1% arabinose). **j**, Psl map from simulations (Psl deposition rate, 5×10^{-5} in dimensionless, arbitrary units (a.u.)). Scale bars, 10 μm.

The importance of Psl in determining this global pattern of bacterial surface exploration can be seen in the visit histograms of the $\Delta P_{psl}/P_{BAD}$-*psl* mutant strain (strain defined in Supplementary Methods), which uses an arabinose-inducible promoter to control Psl production[25]. As the concentration of arabinose in the growth medium was changed from 0% to 1% (w/v), the visit histograms showed a systematic shift from a more uniform distribution of surface visits (that is, having a steep power-law decay) to a more hierarchical distribution (that is, having a broader range of visit frequencies) (Fig. 2d), as evidenced by the change in the effective power-law exponent from -3.3 ± 0.1 to -1.9 ± 0.1, which correspond to low and high arabinose-induced Psl production, respectively. Because the total number of visits is the same for the different curves, a less steep power-law behaviour implies that with increasing Psl concentration the bacterial visits become concentrated in a smaller fraction of the surface. These observations lead us to propose that the higher the Psl concentration for a given surface region, the more likely it is that this region will be visited by more bacteria, causing further local accumulation of Psl and resulting in positive feedback.

Type IV pili (TFP) have a pivotal role in *P. aeruginosa* surface motility and the power-law exploratory mechanism. TFP can extend considerably from the cell body[26] and assist in 'exploring' surface areas beyond the cellular 'footprint'. We propose that TFP associate with Psl-rich surface regions and pull the cell towards these regions with higher probability. Consistent with this, we show that a Δ*pilA* mutant strain, which eliminates TFP-driven twitching motility, results in a drastic reduction of surface exploration (Supplementary Fig. 7). Because cells can secrete Psl as well as associate with Psl, twitching motility effectively promotes positive feedback. Simple track following is just one possible manifestation of this mechanism: cells can approach a given track from any direction. Although such cells can move towards Psl, they do not necessarily reorient themselves tangentially to a given track.

Power-law relationships generally exist only over a limited range in nature and are often difficult to distinguish from other, quantitatively similar relationships. Therefore, rather than concentrating on the approximate power law in the visit frequency distribution and the range over which it is observed, we focused instead on obtaining a deeper quantitative understanding of the processes that generate its functional form. Thus, we performed computer simulations of Psl-guided motility of Psl-secreting bacteria using experimentally measured parameters to test stringently the quantitative interplay between progressive Psl secretion, surface motility and the idea of surface exploration guided by positive feedback.

Bacteria were modelled as non-overlapping line segments in a two-dimensional domain that, when unbiased by Psl, move according to a velocity distribution extracted from the experimental data for $\Delta P_{psl}/P_{BAD}$-*psl* at 0% arabinose. In each step, a fixed amount of Psl was secreted and the bacterial displacement was biased by the local Psl distribution. The bacterial concentration and dimensions as well as the sampling rate were all chosen in accordance with the experimental parameters (Supplementary Methods). The simulations captured the complex distributions from experiments, in both the power-law regime and beyond (Figs 2e and 3c), including the dependence on Psl. The simulated visit frequency distributions exhibited a power-law behaviour that agrees quantitatively with the tracked microscopy data. This is a striking confirmation of the role of Psl-biased motion as the underlying mechanism, because unbiased motion would give rise to non-localized, random-walk-type behaviour. As the Psl production rate was increased for both experiments (Fig. 2d) and simulations (Fig. 2e), the exponents increased over the same numerical range, from −3.1 to −1.8, confirming the shift to more hierarchical distributions in which the number of highly visited sites increased at the expense of many of the rarely visited sites (Fig. 2f–h). Likewise, both the lectin-stained

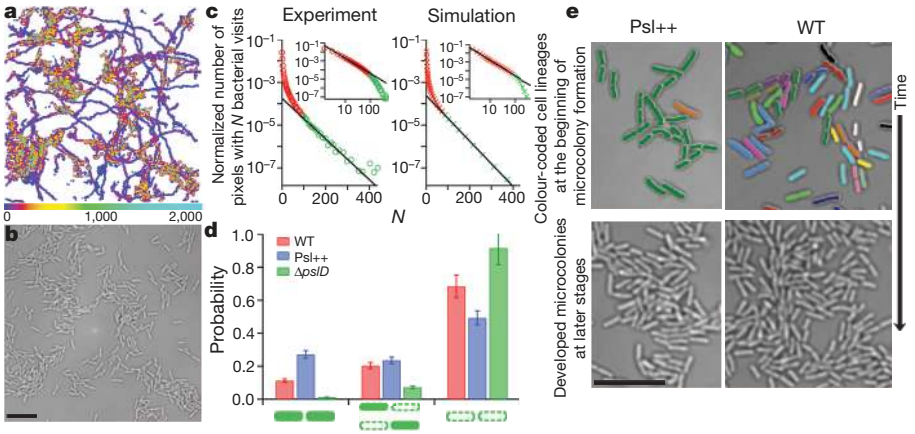

Figure 3 | Local Psl levels determine post-division cell fates. **a**, Visit frequency map of Psl++ for the first 14 h after inoculation. Microcolonies have already started to form. **b**, Bright-field image for Psl++ at $t \approx 14$ h. **c**, Visit frequency distributions of Psl++ from **a** for experiments (left) and simulations (right) agree. The solid line is an exponential fit to the second part of the data (green). Inset, power-law fit to the first part of the data (red). **d**, Probability of post-division cells' fates: stay (filled rod), leave (open dashed rod), wild type (red), Psl++ (blue), Δ*pslD* (green). Error bars are estimated from $1/\sqrt{N_{\mathrm{div}}}$, where N_{div} is the total number of division events during the time period of interest ($N_{\mathrm{div}} \geq 90$). **e**, Wild-type and Psl++ microcolonies have drastically different compositions, as depicted by colour-coded cell division lineages at early stages of microcolony formation (top row). For Psl++ the microcolony is dominated by a single lineage, whereas the wild-type microcolony has 20 different lineages. The bottom row depicts more developed microcolonies at the same location 3.3 h later. Scale bars, 10 μm.

Psl image observed in experiments (Fig. 2i) and the simulated Psl map (Fig. 2j) showed the hierarchical nature of the spatial distribution of Psl.

Power laws (such as Zipf's law[17,18] or its continuous generalization, Pareto distributions) are known to describe self-organized systems like the wealth distributions in capitalist economies[18]. We found that bacteria are guided by synergistic rich-get-richer mechanisms. Both simulations and experiments indicate that the ability of *P. aeruginosa* to secrete Psl and its tendency to associate with Psl result in an exploratory strategy by which cells go where other cells go most often. (The range of exponents we observe here for bacteria is essentially the same as for income distributions[27].) This strategy results in a small number of cells being positioned at locations that are extremely enriched in communally produced Psl. This arrangement provides the conditions necessary for microcolony growth. Notably, these effects persist even when we completely turn off cell division in computer simulations, which indicates that the distribution of cells is a consequence of their exploratory strategy rather than of growth.

We examined the behaviour of bacterial communities beyond the power-law exploratory phase to show how growth can amplify differences in cell density on the surface caused by exploration. We found that high local Psl concentrations resulted in discrete microcolonies that exhibit localized exponential growth rather than delocalized surface exploration. For data on wild type (Fig. 2a–c), the power-law behaviour persisted only in the initial exploratory phase when there were no microcolonies. In fact, small deviations from the power law can be observed in the lower right portion of Fig. 2c (green arrow), which corresponds to highly visited areas with the highest local Psl concentrations. To examine community behaviour near high Psl concentrations, we examined the $\Delta P_{psl}/P_{BAD}$-*psl* mutant that overproduces Psl in the presence of 1% arabinose (Psl++). The bacterial visit frequency map for the Psl++ cells was significantly different from that of wild-type cells (Fig. 3a). Compared with Fig. 2a, there are far fewer tracks leading into and out of the cellular aggregates in Fig. 3a, implying that few cells joined or departed from these aggregates. The regions of highest numbers of bacterial visits in the map fully correlate with the existence of microcolonies of closely packed bacteria in the bright-field image (Fig. 3b). The cell densities in the highly visited areas were more than three times higher than the average cell density on the surface. Moreover, the Psl++ cells formed microcolonies earlier than did the wild-type cells. Notably, owing to microcolony formation, a portion of the visit frequency distribution is described by an exponential rather than a power law in both experiments and simulations (Fig. 3c).

We used cell tracking to show that the exponential growth which enables localized microcolony formation is ultimately rooted in how local Psl concentrations determine post-division cell fates. We distinguished three possibilities: the post-division cells both stay near the division event, both leave (see definitions of 'stay' and 'leave' in Supplementary Methods) or one cell stays and the other leaves. Figure 3d shows the probabilities of these cell fates observed for wild type, Psl++ and Δ*pslD*. The probability of both cells staying for the Psl++ mutant was approximately three times as high as for wild type. In contrast, the probability of both cells staying for the Δ*pslD* mutant strain was essentially zero. In fact, the fraction of total population growth due to cell division (as opposed to motile cells joining the microcolony, cells attaching from solution and so on) was ~85% for the Psl++ mutant, which directly leads to an exponential visit distribution (Supplementary Fig. 8). We traced the division lineage of cells in developing microcolonies (Fig. 3e). The Psl++ microcolony was derived mostly from a single lineage, consistent with our proposal that such cells primarily divide and remain in the same area owing to the high local Psl concentrations. In contrast, the wild-type microcolony developed from many cell lineages as a result of the initial power-law exploratory phase. (More examples can be found in Supplementary Figs 9 and 10.) These data strongly support our rich-get-richer model for microcolony formation.

The results presented here quantitatively show the key steps important for the transition from surface attachment and surface exploration to microcolony formation: the evolving distribution of Psl on a solid surface provides a mechanism for bacteria to self-organize socially, resulting in a rich-get-richer power-law distribution of visit frequencies and a hierarchical distribution of Psl concentrations on the surface. This in turn results in a small number of aggregated cells becoming highly enriched in Psl, which enables them to serve as the founding population for localized exponential growth and the formation of microcolonies that ultimately evolve into the mushroom-like 'stalks-and-caps' morphology of mature biofilms[4–6].

METHODS SUMMARY

Wild-type *P. aeruginosa* strain PAO1[28] and its isogenic mutants Δ*pslD*, $\Delta P_{psl}/P_{BAD}$-*psl*[14] and Δ*pilA* were used in this study. The growth rates of the strains are nearly identical (to within measurement error; Supplementary Fig. 1). For $\Delta P_{psl}/P_{BAD}$-*psl*, arabinose was used to control Psl production[14]. FAB medium[29]

with 0.6 mM glutamate was used for flow cell experiments, which were conducted at 30 °C with a flow rate of 3 ml h^{-1}. Flow cells were assembled as previously described[30]. The flow was stopped for bacterial inoculation and 20 min of incubation, and then resumed with the initiation of image recording.

Images were made with an Olympus microscope. Bright-field images were recorded every 3 s. Each data set, which had 18,000–48,000 frames, contained up to 1,000,000 bacteria images. Psl was stained with 100 μg ml^{-1} TRITC-labelled *Hippeastrum* hybrid lectin from amaryllis[12]. The image size was 67 μm × 67 μm (1,024 × 1,024 pixels).

In simulations, line segments (representing bacteria) moved within a square surface window with periodic boundary conditions. Each bacterium moved with fixed step size at a variable angle deviating from its cell body axis according to distributions drawn from experiments, and deposited Psl at its centre at a tunable rate. This Psl in turn modified the bacterial motion through Psl-concentration-based biasing. In addition, random reorientations happened at a prescribed rate in accordance with the bacterial mean square displacement from experiments, influenced by Psl. The total simulation time was chosen such that the final visit count was the same as in experiments.

Full Methods and any associated references are available in the online version of the paper.

Received 19 September 2012; accepted 8 April 2013.
Published online 8 May 2013.

1. Costerton, J. W., Stewart, P. S. & Greenberg, E. P. Bacterial biofilms: a common cause of persistent infections. *Science* **284,** 1318–1322 (1999).
2. O'Toole, G. A. & Kolter, R. Flagellar and twitching motility are necessary for *Pseudomonas aeruginosa* biofilm development. *Mol. Microbiol.* **30,** 295–304 (1998).
3. O'Toole, G., Kaplan, H. B. & Kolter, R. Biofilm formation as microbial development. *Annu. Rev. Microbiol.* **54,** 49–79 (2000).
4. Stoodley, P., Sauer, K., Davies, D. G. & Costerton, J. W. Biofilms as complex differentiated communities. *Annu. Rev. Microbiol.* **56,** 187–209 (2002).
5. Klausen, M., Aaes-Jørgensen, A., Molin, S. & Tolker-Nielsen, T. Involvement of bacterial migration in the development of complex multicellular structures in *Pseudomonas aeruginosa* biofilms. *Mol. Microbiol.* **50,** 61–68 (2003).
6. Davies, D. G. *et al.* The involvement of cell-to-cell signals in the development of a bacterial biofilm. *Science* **280,** 295–298 (1998).
7. Mann, E. E. & Wozniak, D. J. Pseudomonas biofilm matrix composition and niche biology. *FEMS Microbiol. Rev.* **36,** 893–916 (2012).
8. Lyczak, J. B., Cannon, C. L. & Pier, G. B. Establishment of *Pseudomonas aeruginosa* infection: lessons from a versatile opportunist. *Microbes Infect.* **2,** 1051–1060 (2000).
9. Tatterson, L. E., Poschet, J. F., Firoved, A., Skidmore, J. & Deretic, V. CFTR and pseudomonas infections in cystic fibrosis. *Front. Biosci.* **6,** d890–897 (2001).
10. Singh, P. K. *et al.* Quorum-sensing signals indicate that cystic fibrosis lungs are infected with bacterial biofilms. *Nature* **407,** 762–764 (2000).
11. Friedman, L. & Kolter, R. Two genetic loci produce distinct carbohydrate-rich structural components of the *Pseudomonas aeruginosa* biofilm matrix. *J. Bacteriol.* **186,** 4457–4465 (2004).
12. Ma, L. Y., Lu, H. P., Sprinkle, A., Parsek, M. R. & Wozniak, D. J. *Pseudomonas aeruginosa* Psl is a galactose- and mannose-rich exopolysaccharide. *J. Bacteriol.* **189,** 8353–8356 (2007).
13. Byrd, M. S. *et al.* Genetic and biochemical analyses of the *Pseudomonas aeruginosa* Psl exopolysaccharide reveal overlapping roles for polysaccharide synthesis enzymes in Psl and LPS production. *Mol. Microbiol.* **73,** 622–638 (2009).
14. Ma, L., Jackson, K. D., Landry, R. M., Parsek, M. R. & Wozniak, D. J. Analysis of *Pseudomonas aeruginosa* conditional psl variants reveals roles for the psl polysaccharide in adhesion and maintaining biofilm structure postattachment. *J. Bacteriol.* **188,** 8213–8221 (2006).
15. Byrd, M. S., Pang, B., Mishra, M., Swords, W. E. & Wozniak, D. J. The *Pseudomonas aeruginosa* exopolysaccharide Psl facilitates surface adherence and NF-κB activation in A549 cells. *mBio* **1,** e00140–10 (2010).
16. Gibiansky, M. L. *et al.* Bacteria use type IV pili to walk upright and detach from surfaces. *Science* **330,** 197 (2010).
17. Newman, M. E. J. Power laws, Pareto distributions and Zipf's law. *Contemp. Phys.* **46,** 323–351 (2005).
18. Gabaix, X. Power laws in economics and finance. *Annu. Rev. Econ.* **1,** 255–294 (2009).
19. Eagon, R. G. Composition of an extracellular slime produced by *Pseudomonas aeruginosa*. *Can. J. Microbiol.* **8,** 585–586 (1962).
20. Sutherland, I. W. The biofilm matrix: an immobilized but dynamic microbial environment. *Trends Microbiol.* **9,** 222–227 (2001).
21. Whitchurch, C. B., Tolker-Nielsen, T., Ragas, P. C. & Mattick, J. S. Extracellular DNA required for bacterial biofilm formation. *Science* **295,** 1487 (2002).
22. Colvin, K. M. *et al.* The Pel and Psl polysaccharides provide *Pseudomonas aeruginosa* structural redundancy within the biofilm matrix. *Environ. Microbiol.* **14,** 1913–1928 (2012).
23. Monroe, D. Looking for chinks in the armor of bacterial biofilms. *PLoS Biol.* **5,** e307 (2007).
24. Flemming, H. C., Neu, T. R. & Wozniak, D. J. The EPS matrix: the "house of biofilm cells". *J. Bacteriol.* **189,** 7945–7947 (2007).
25. Newman, J. R. & Fuqua, C. Broad-host-range expression vectors that carry the l-arabinose-inducible *Escherichia coli araBAD* promoter and the *araC* regulator. *Gene* **227,** 197–203 (1999).
26. Skerker, J. M. & Berg, H. C. Direct observation of extension and retraction of type IV pili. *Proc. Natl Acad. Sci. USA* **98,** 6901–6904 (2001).
27. Solomon, S. & Richmond, P. Power laws of wealth, market order volumes and market returns. *Physica A* **299,** 188–197 (2001).
28. Holloway, B. W. Genetic recombination in *Pseudomonas aeruginosa*. *J. Gen. Microbiol.* **13,** 572–581 (1955).
29. Heydorn, A. *et al.* Experimental reproducibility in flow-chamber biofilms. *Microbiology* **146,** 2409–2415 (2000).
30. Sternberg, C. & Tolker-Nielsen, T. Growing and analyzing biofilms in flow cells. *Curr. Protocols Microbiol.* **21,** 1B.2.1–1B.2.17 (2006).

Supplementary Information is available in the online version of the paper.

Acknowledgements K.Z., B.S.T., M.R.P. and G.C.L.W. are supported by the US National Institutes of Health (NIH 1RO1HL087920). K.Z. and G.C.L.W. also acknowledge support from the US National Science Foundation (NSF DMR1106106) and a UCLA Transdisciplinary Seed Grant. B.S.T., J.J.H. and M.R.P. also acknowledge support from the NIH (R01AI077628, R01AI081983, R56AI061396) and NSF (MCB0822405). B.S.T. is supported by the Cystic Fibrosis Foundation Postdoctoral Fellowship (TSENG11F0). J.J.H. was supported by a postdoctoral fellowship from the Natural Sciences and Engineering Research Council of Canada. B.B. and E.L. acknowledge support from the NSF under DMR-1006430 (E.L.) and DGE-0824162 (B.B.). The authors would like to thank J. Copic for discussions and R. J. Siehnel for technical assistance. We dedicate this paper to the memory of M. Shannon.

Author Contributions G.C.L.W., M.R.P. and K.Z. conceived the project. K.Z., B.S.T., M.R.P. and G.C.L.W. designed studies. K.Z. and B.S.T. performed experimental measurements. K.Z. and G.C.L.W. performed image analysis. F.J. helped in performing image analysis. M.L.G. helped in collecting experimental data. B.S.T., J.J.H. and M.R.P. constructed strains. B.B. and E.L. designed the model and performed computer simulations. K.Z., B.S.T., B.B., E.L., M.R.P. and G.C.L.W. wrote the paper. All authors discussed the results and commented on the manuscript.

Author Information Reprints and permissions information is available at www.nature.com/reprints. The authors declare no competing financial interests. Readers are welcome to comment on the online version of the paper. Correspondence and requests for materials should be addressed to G.C.L.W. (gclwong@seas.ucla.edu), M.R.P. (parsem@u.washington.edu) or E.L. (luijten@northwestern.edu).

METHODS

Strains and growth conditions. *Pseudomonas aeruginosa* strain PAO1 wild type[28] and its isogenic mutants Δ*pslD*, the *psl*-inducible strain $\Delta P_{psl}/P_{BAD}$-*psl* and Δ*pilA* were used in this study. The growth rates of the strains were nearly identical (to within measurement error; Supplementary Fig. 1). For strain $\Delta P_{psl}/P_{BAD}$-*psl*, different amounts of arabinose (Sigma-Aldrich; 1%, 0.1% and 0.005% were used in this work) were added into the medium to control the production of Psl[14].

FAB medium[29] with 0.6 mM glutamate (Sigma-Aldrich) as the carbon source was used for flow cell experiments. An inoculum was prepared by growing strains in test tubes containing FAB with 30 mM glutamate, shaking at 220 r.p.m. and 37 °C to D_{600nm} ~0.5. Cultures were then diluted to D_{600nm} ~0.01 in FAB medium with 0.6 mM glutamate, which was used for injection into the flow chamber.

Flow cell assembly, sterilization and washing of the system. The flow cell was purchased from the Department of Systems Biology, Technical University of Denmark and assembled as previously described[30]. The assembled flow cell was connected to a syringe through a 0.22-μm filter (Fisher Scientific) using silicon tubing (Dow Corning). Then the whole system was sterilized overnight with 3% H_2O_2 (Fisher Scientific) at 3 ml h^{-1} using a syringe pump (KD Scientific). After the sterilization, autoclaved, deionized water was used to wash the whole system overnight. The system was washed again using FAB medium with 0.6 mM glutamate before starting the inoculation of the bacteria into the flow cell. The flow was stopped for bacterial inoculation and 20 min of incubation, and then resumed with the initiation of image recording. Different flow rates have recently been reported to have an effect on bacterial surface behaviour[31], and it will be interesting to using large-scale tracking methods in this context. In this work, the flow cell experiments were conducted at 30 °C with a flow rate of 3 ml h^{-1}.

Data acquisition. The images were made using an EMCCD camera (Andor iXon) using IQ software (Andor) on an Olympus IX81 microscope equipped with Zero Drift autofocus system. The bright-field images were recorded every 3 s for a total recording time of about 20 h (varying by strain). Each data set, which had 18,000–48,000 frames, contained up to 1,000,000 bacteria images. The image size is 67 μm × 67 μm (1,024 × 1,024 pixels).

Lectin staining. The Psl trails left by bacteria were stained with TRITC-labelled *Hippeastrum* hybrid (amaryllis) (HHA) lectin (EY laboratories)[12]. Flow was suspended and 0.3 ml of 100 μg ml^{-1} TRITC-HHA in FAB medium with 0.6 mM glutamate was injected upstream of the inlet flow. During the injection, the flow chamber was monitored through the camera to make sure there was no shift or disturbance of the stage due to injection. The flow chamber was stained for 15 min without flow and then washed for 15 min with flow at a flow rate of 3 ml h^{-1} in the dark before imaging.

Image analysis, surface coverage map and visit frequency map. Images were analysed as previously described[16]. In Fig. 1a–e, we used the area of each moving cell to generate the surface coverage from the bacterial trajectories. The visit frequency distributions are generated at full data resolution; for the visit maps, we used the centre of the cell to mark the trail, and spread each of these marks over a square patch eight pixels (~0.5 μm) wide, in accordance with bacterium width. The distribution of Psl on the PAO1 surface is expected to be more complex[32], but this will amount to a more complex point spread function and is not expected to alter the results qualitatively.

Simulation of Psl-guided motility of Psl-secreting bacteria. The computer simulations used a two-dimensional model in which an exponentially growing number of line segments of unit length moved within a square, periodic domain of side length 35, approximately corresponding to the experimental viewing window. Each bacterium was assigned a fixed step size and stepped with a variable angle. Both the step size and the stepping angle were drawn from the experimentally determined motion distribution for the $\Delta P_{psl}/P_{BAD}$-*psl* strain at an arabinose concentration of 0% (that is, in the absence of Psl). Starting from a random non-overlapping configuration, all bacteria propagated in discrete time steps ($\Delta t = 3$ s), either moving at their constant, assigned rate, keeping their director fixed, or randomly reorienting. Reorientations occurred at a frequency 3.7%, determined by the mean squared displacement of the bacteria in the experiment. The effect of arabinose was represented by letting each bacterium deposit Psl at its centre at a tunable rate. The surface accumulation of Psl was recorded in elementary squares of side length 1/29 (corresponding to the experimental pixel size). The motion was in turn biased according to the presence of Psl within the vicinity of the leading pole of the bacterium. The total simulation time was chosen such that the final visit count was the same as in experiments. Over this window, we sampled individual bacterial trajectories as well as visit frequencies of all pixels (Supplementary Methods).

31. Lecuyer, S. *et al.* Shear stress increases the residence time of adhesion of *Pseudomonas aeruginosa*. *Biophys. J.* **100,** 341–350 (2011).
32. Ma, L. *et al.* Assembly and development of the *Pseudomonas aeruginosa* biofilm matrix. *PLoS Pathog.* **5,** e1000354 (2009).